Liquid Film Flow on Structured Wires: Fluid Dynamics and Gas-Side Mass Transfer

J. Grünig, S.-J. Kim, and M. Kraume
Dept. of Process Engineering, Chair of Chemical and Process Engineering, Technische Universität Berlin, Straße des 17, Juni 135, D-10623 Berlin, Germany

DOI 10.1002/aic.13795
Published online April 4, 2012 in Wiley Online Library (wileyonlinelibrary.com).

The liquid film flow on different structured wires and chains is observed experimentally to assess the suitability of a structured packing consisting of vertical wires. The results show that liquid beads as they appear on cylindrical wires are inhibited by certain chain geometries. This increases the flooding gas load up to $F = 12\ Pa^{0.5}$. As the stabilized film shows no liquid bead motion, the liquid velocity at the interface is less which results in lower gas-side mass-transfer coefficients. An estimation of the packing characteristics for different chain geometries with an assumed wire packing density of 40,000 wires/m^2 is made. The interfacial area, mass-transfer coefficients, and consequently the separation efficiency strongly depend on the liquid load. However, the proposed gas-side separation efficiencies are slightly lower compared to common structured packings but the advantages are higher load limits, a better liquid distribution, and lower pressure drop. © 2012 American Institute of Chemical Engineers *AIChE J,* 59: 295–302, 2013
Keywords: wetted wire packing, structured wires, fluid dynamics, mass transfer

Introduction

Packed columns are used for various separation problems in the chemical industry. Nowadays, there are plenty of different dumped and structured packings available.

Modern corrugated sheet structured packings (CSSPs) were developed in the 1960s[1] and offer high-separation efficiencies at moderate pressure drop but suffer maldistribution of liquid and gas phase, so the liquid has to be redistributed after a certain height.[2]

The concept of the wetted wire packing proposed by Hattori et al.[3] has promise to have a uniform phase distribution in the whole packing and a low-specific pressure drop. It mainly consists of parallel wire elements which are individually supplied with liquid from a special liquid distributor. Therefore, the liquid is forced to run on defined flow paths and no radial liquid flow occurs that could lead to maldistribution.

This study examines this concept regarding the fluid dynamics and mass transfer of one representative packing element. On the one hand, one gets detailed information which effects occur inside the packing and, on the other hand, one is able to estimate the packing performance from the single wire data.

In previous investigations,[4] a single cylindrical wire with a diameter of 1 mm was examined. It revealed that the film has a certain pattern of liquid beads running over a thin basis film. This raised the question, if the bead formation could be suppressed by structured wire geometry and how this would affect the fluid dynamics and the mass transfer. Therefore, different structured wire and chain geometries were observed for their suitability as packing element.

Correspondence concerning this article should be addressed to J. Grünig at jochen.gruenig@tu-berlin.de.

Materials and Methods

Experimental setup

The flow sheet of the experimental setup is shown in Figure 1. The main element is a vertical glass channel with a quadratic cross-sectional area of $20 \times 20\ mm^2$ and a length of 1 m. The examined structured wires and chains are fixed in its center. Water is pumped from a storage tank to the top of the channel. The liquid is distributed on the wire inside the channel top and flows down as a film and gets into contact with the gas phase. At the channel bottom, the liquid is collected and fed back into the storage tank. Air is guided into the bottom of the channel and flows upward counter currently to the liquid film before it exits into the environment. The inlet temperatures of liquid and gas phase are regulated by heaters and measured at the inlet and outlet of the channel. A high-speed camera and a synchronized lighting are used to detect the film thickness at different vertical positions. The analysis of the images is automated with an image recognition software tool. A more detailed description of the test facility and the optical measurement methods is given by Grünig et al.[4]

Investigated structured wires

In a preliminary test, five different structured wires were screened concerning their film flow behavior. Table 1 gives an overview of the properties of the investigated structured wires. In the following, it will be motivated why these wires were chosen. Eventually, it emerged that not all wires met

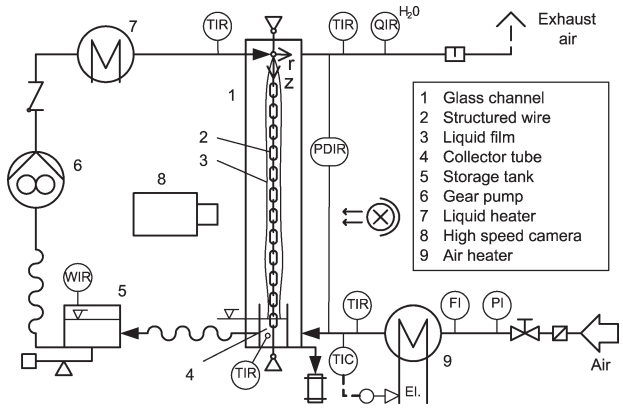

Figure 1. Sketch of experimental setup.

the requirements to be used as packing element, namely, the locking wire and the knitted wire braid.

After studying the film flow on a cylindrical wire, there was the idea to influence the film by attaching trip wires on the central wire. Among commercially available wires, locking wires have a structure that comes close to that idea: A thin wire spirally entwines around a thick central wire (see Table 1). First tests revealed although that the liquid beads did still appear and were not decelerated significantly. However, due to the spiral structure of the wire, the beads began to spin eccentrically around the wire and were thrown-off after a certain running length. As it is not desired to have free droplets in the packing, which can be entrained by the gas flow, this wire was no longer considered.

A further consideration was to have a wire, which stabilizes the film flow by a surrounding structure. Therefore, a knitted wire braid (Rhodius GmbH, Germany) was applied which wrapped a central wire of 1 mm diameter (see Table 1). It revealed that the film flows mainly inside the wire structure and no liquid beads could be observed. Because of the dense knitted wire structure, the effective film surface could not be determined with the optical method. However, the mass-transfer rates indicated that the outer surface is not wetted completely, and thus, the effective interfacial area is lower. For this reason, the knitted wire braid was also excluded from further investigations.

The idea behind the investigation of chains was that the transition between the chain links hinders the bead motion which stabilizes the film.

Load limits

The load limits were defined as the flooding point and were observed visually. At a fixed liquid load, the gas load was continuously increased until the point was reached where the liquid reversed its flow direction as it was completely transported upward by the gas flow.

Film dimension measurements and interfacial area estimation

The experimental methods are explained in detail by Grünig et al.[4] As the wire geometries differed from the previous cylindrical wire, the optical measurement of the film thickness and the estimation of the interfacial area had to be adapted and are explained below.

The local film dimension is measured at three different vertical positions of the channel. In the case of the armor chain, it was oriented with the flat side to the camera. Because the chains have complex geometries, an unambiguous film thickness as for the cylindrical wire cannot be determined. Therefore, the film dimension is observed at distinctive positions of the chain links as shown in Figures 2a–c. The interfacial area was estimated by means of a geometric model of the liquid film. The geometric data was obtained from the film dimension measurements. The volumetric model was established for each chain individually, as the liquid film had a different shape.

Watch Chain. The film geometry is approximated with ellipsoids that are placed in the chain links which have the dimensions of the lengths l_1 and l_2 of the chain link and the film dimension e_1 (see Table 1 and Figure 2). The surface

Table 1. Properties of Investigated Structured Wires and Chains

Material	Locking Wire Brass	Knitted Wire Braid Stainl. steel	Watch Chain Brass	Armor Chain Brass	Bead Chain Nickel-plated steel
Dimensions, mm	$l_1 = 1.7$	$d_1 = 4$	$l_1 = 5.6$ $l_2 = 3.5$	$l_1 = 3.1$ $l_2 = 3.8$	$l_1 = 3.6$ $d_1 = 2.4$
Wire diameter d_W, mm	0.5/0.3	0.12	0.8	1	0.6
Specific area $\tilde{a}_W$, 10^3 mm^2/m	3.30	30.5	7.10	12.8	5.55
Cross-sectional area $A_{CSA,W}$, mm^2	0.33	0.91	1.42	3.19	2.13

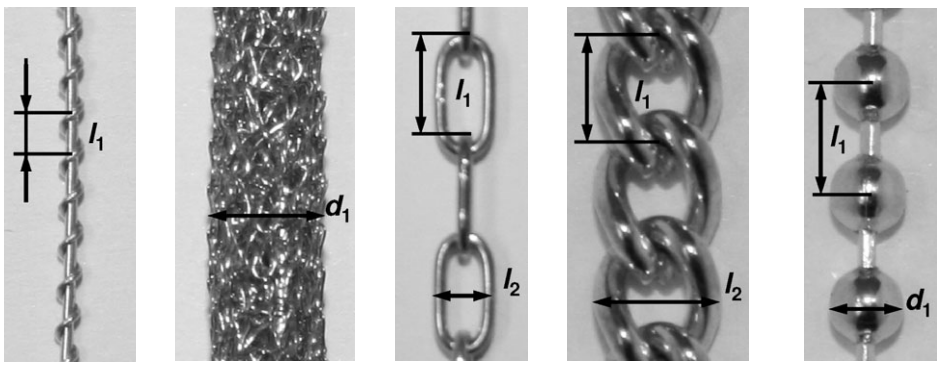

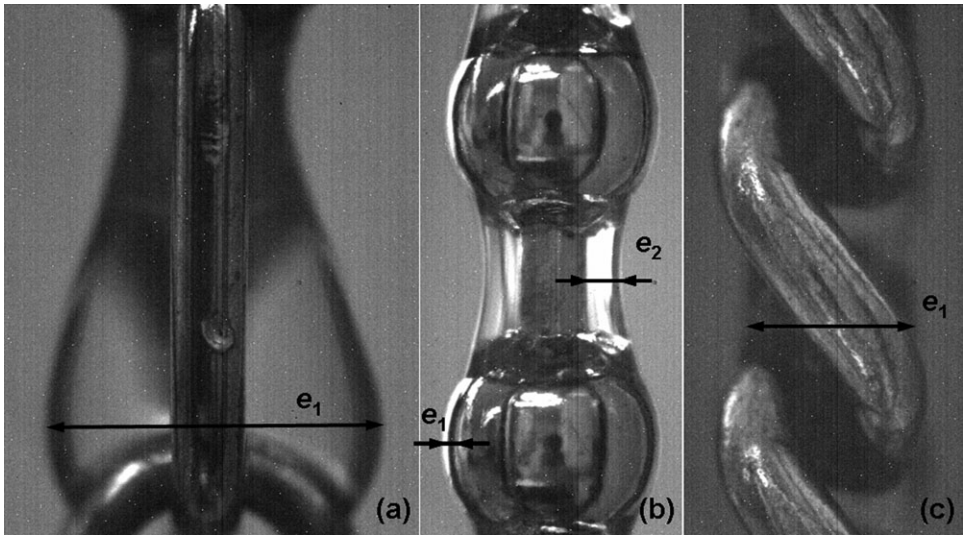

Figure 2. Measured film dimensions on (a) watch chain, (b) bead chain, and (c) armor chain.

area of an ellipsoid can be approximated (max. relative error 1.2%) with the Knut Thomsen formula[5] as

$$A_{\text{ellipsoid}} = 4\pi \left(\frac{(ab)^{1.6}(ac)^{1.6}(bc)^{1.6}}{3} \right)^{0.625} \tag{1}$$

and the volume can be calculated as

$$V_{\text{ellipsoid}} = \frac{4}{3}\pi\, abc \tag{2}$$

By summarizing the surface of the ellipsoids and referring the total surface area to the length of the chain, one obtains

$$\tilde{a}_{\text{l,W}} = 4\pi \left(\frac{\left(\frac{l_1}{2}\frac{l_2}{2}\right)^{1.6} \left(\frac{l_1}{2}\frac{e_1}{2}\right)^{1.6} \left(\frac{l_2}{2}\frac{e_1}{2}\right)^{1.6}}{3} \right)^{0.625} \frac{N_{\text{CL}}}{L_{\text{W}}} \tag{3}$$

The liquid holdup is calculated as the total volume of the ellipsoids less than the chain volume referred to the length of the chain

$$HU_{\text{l,W}} = \frac{4}{3}\pi \frac{l_1}{2}\frac{l_2}{2}\frac{e_1}{2}\frac{N_{\text{CL}}}{L_{\text{W}}} - A_{\text{CSA,W}} \tag{4}$$

Bead Chain. As the film flows over the solid beads, the film appears as rotationally symmetric body with a sinusoidal surface undulation. The profile curve is, therefore, approximated by a sinus function

$$f(x) = A\, \sin(C\, x) + D \tag{5}$$

The film dimension measurements deliver the amplitude A and the offset D of the function, whereas the period length C is determined by the chain link length l_1

$$A = \frac{e_1 - e_2}{4} \quad D = \frac{e_1 + e_2}{4} \quad \text{and} \quad C = \frac{2\pi}{l_1} \tag{6}$$

The lateral area of an axially symmetric body defined by a function can be calculated according to Guldins law, as the arc length of the function times the length of the path of the center of mass of the function. The arc length of the sinus function is approximated by the arithmetic mean of two polygons in which the sinus function is inscribed

$$L_{\text{sin}} = \frac{1}{2}\left[4\sqrt{\left(\frac{l_1}{8}\right)^2 + \left(\frac{e_1 - e_2}{4}\right)^2} + 2\frac{l_1}{4} + 4\sqrt{\left(\frac{l_1}{4}\right)^2 + \left(\frac{e_1 - e_2}{4}\right)^2} \right] \tag{7}$$

The path of the center of mass of the sinus function is a circle with the offset D as the radius. Thus, the specific surface area is calculated as

$$\tilde{a}_{\text{l,W}} = 2\pi D\, L_{\text{sin}} \frac{1}{l_1} \tag{8}$$

and the liquid holdup as

$$HU_{\text{l,W}} = \left[\pi \left(\frac{A^2 l_1}{2} + D^2 l_1 \right) - \left(\frac{\pi}{6} d_1^3 + \frac{\pi}{4} d_{\text{w}}^2 (l_1 - d_{\text{W}}) \right) \right] \frac{1}{l_1} \tag{9}$$

For the comparison of the different geometries, a flat sheet film thickness and a film velocity were defined as

$$\delta_{\text{m}} = \frac{HU_{\text{l,W}}}{\tilde{a}_{\text{W}}} \quad \text{and} \quad \bar{w}_{\text{l,f}} = \frac{\dot{V}_{\text{l,W}}}{HU_{\text{l,W}}} \tag{10}$$

Armor Chain. The liquid film on the armor chain appears to be a streak with no bead formation. Therefore, its geometry was approximated as a cylinder with elliptic base area. One axis of the ellipse is the measured film dimension, the second axis is regarded as the width l_2 (see Table 1) of the armor chain. Then, the length specific surface area calculates as the circumference of the ellipse

$$\tilde{a}_{\text{l,W}} = \pi \sqrt{2\left(\left[\frac{e_1}{2}\right]^2 + \left[\frac{l_1}{2}\right]^2 \right)} \tag{11}$$

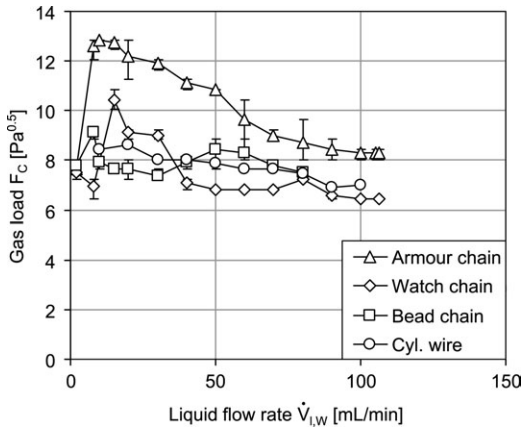

Figure 3. Load limits at flooding point depending on the liquid flow rate for different wires.

Error bars: minimum and maximum values.

In similar manner, the liquid holdup is calculated as

$$HU_{l,W} = \pi \frac{l_1}{2} \frac{e_1}{2} - A_{CSA,W} \tag{12}$$

Liquid holdup

The liquid holdup is measured with the shut-off method. As the liquid circuit is shut off, the remaining liquid mass on the wire drains into the storage tank. This causes a jump of the storage tank weight which is recorded by an electronic balance. The height of the jump can be related to the liquid holdup.

Gas-side mass transfer

To determine the gas-side mass transfer, the increase of the humidity of the gas due to evaporation of the liquid was measured at the inlet and outlet of the channel. A mass balance leads to the molar evaporation flow rate as

$$\dot{N}_{H_2O} = \dot{N}_{g,in} \frac{y_{H_2O,out} - y_{H_2O,in}}{1 - y_{H_2O,out}} \tag{13}$$

The calculation of the gas-side mass-transfer coefficient was carried out similar to the method presented by Gilliland and Sherwood.[6] In consideration of the Stefan diffusion, the gas-side mass-transfer coefficient is calculated as

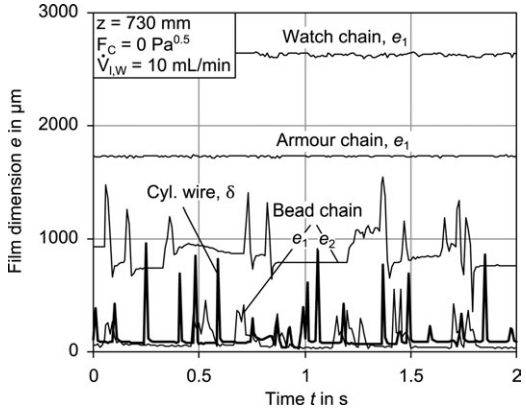

Figure 4. Recording of the local film dimensions.

$$\beta_g = \frac{\dot{N}_{H_2O} R T_g}{p \tilde{a}_{l,W} L_W} \cdot \frac{p_{air,m}}{\Delta p_{H_2O,ln}} \quad \text{with}$$

$$p_{air,m} = p - \frac{p_{H_2O,I,in} + p_{H_2O,I,out} + p_{H_2O,in} + p_{H_2O,out}}{4} \tag{14}$$

The partial pressures at the interphase $p_{H_2O,I,in}$ and $p_{H_2O,I,out}$ are the saturation vapor pressures at liquid temperature and are calculated with the Magnus equation according to VDI/VDE 3514 guideline.[7]

Results and Discussion

Load limits

Figure 3 shows the load limits at flooding depending on the liquid flow rate for different wire geometries. All investigated wire geometries show high-gas load limits which are slightly decreasing with increasing liquid load. It is remarkable that the maximum gas load limit of the armor chain is significantly higher than those of the other wire geometries. The reason lies in the different film flow pattern of the armor chain. At liquid flow rates higher than 8 mL/min bead formation does not occur. Because of the reduced frontal area, the liquid film offers less resistance to the gas flow and the flooding occurs at higher gas loads.

Local film dimensions

The vertical motion of beads as it appears on the cylindrical wire could be suppressed by certain chain geometries. In Figure 4, the local film dimensions of different wire geometries are plotted against time. The watch chain and the armor chain show almost no fluctuation of the local film dimension in time independent of the vertical position. However, the cylindrical wire and the bead chain exhibit significant fluctuations of the local film dimension due to travelling beads.

Although a rising gas load leads to thicker beads for the cylindrical wire, whereas the basis film thickness remains constant, the film dimension of the chains is almost independent of the gas load. Figure 5 shows the film dimension of the chains and the cylindrical wire in dependency of the liquid flow rate at a running length of 330 mm. The measurement data are averaged over the gas load. The standard deviation is below 5%.

The film dimension e_1 of the watch chain is continuously increasing with rising liquid flow rate. This results from the

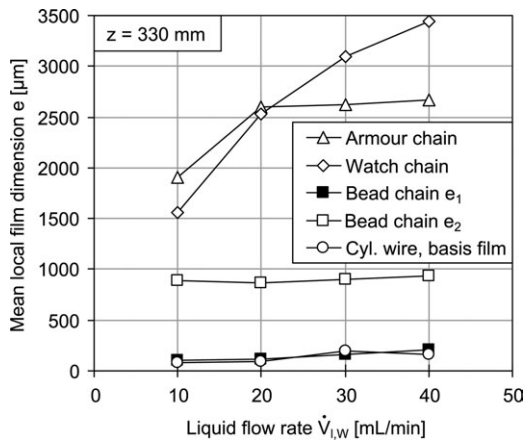

Figure 5. Local film dimensions for different chains and the cylindrical wire depending on the liquid flow rate.

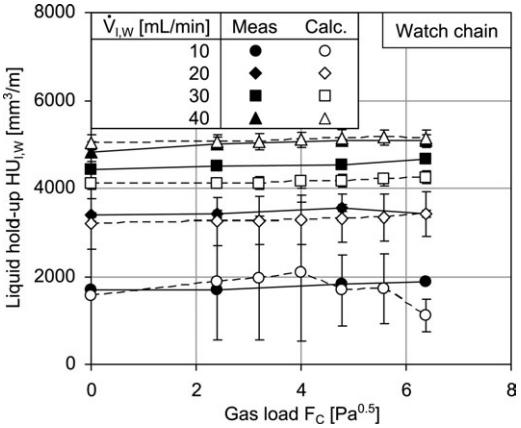

Figure 6. Liquid holdup against the gas load for different liquid flow rates of the watch chain.

Comparison of measured and calculated values. Error bars: minimum and maximum values.

growth of the ellipsoids formed in each chain link. For the armor chain, it can be seen that the slope is less increasing above a liquid flow rate of 20 L/min. This behavior could be caused by the beginning decomposition of the continuous liquid streak leading to higher-liquid film velocities. Another possible cause might be the geometrical expansion in that dimension which is not captured by the camera. The bead chain shows only a slight increase of the film dimension. Although the liquid flow rate is increased, fluctuations occur due to the liquid film and the standard deviation of the temporal film dimension is much higher than of the other chains.

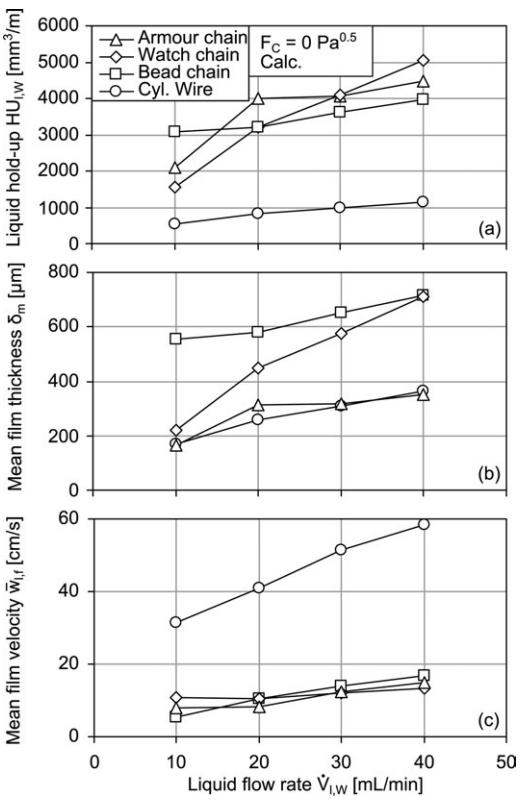

Figure 7. Calculated liquid holdup, mean film thickness, and film velocity for different chains and the cylindrical wire against the liquid flow rate without gas load.

Liquid holdup

In this section, the results of the shut-off method are compared with the calculated liquid holdup values from the film dimension data according to Eqs. 4, 9, and 12. Figure 6 compares both results using the example of the watch chain for different liquid flow rates depending on the gas load. Similar to the film dimension, the liquid holdup shows no dependency of the gas load. This behavior is also typical for packed columns at an operation point below the loading limit. Both the shut-off results and calculated values increase with rising liquid flow rate and are in good agreement. However, the bead and armor chain show significant deviation between measurement and calculation. These chains hold a significant amount of liquid volume in the gaps between the chain links after shutting off the liquid supply, and therefore, this is not detected by the measurement method.

In Figures 7a–c, the calculated liquid holdup, mean film thickness, and mean film velocity (see Eq. 10) are plotted against the liquid flow rate for different chains without gas load. It is obvious that the liquid holdup rises with increasing liquid flow rates for all geometries. However, it also reveals that the liquid holdup of the chains is significantly higher than for the cylindrical wire. The mean film thickness is defined as the liquid holdup referred to the specific dry surface area and can be seen as a measure how effective the given surface is able to retain the liquid. Therefore, its dependency from the liquid load is the same as for the liquid holdup. The armor chain shows similar film thicknesses as the cylindrical wire, whereas the bead chain has significantly higher film thicknesses. However, the watch chain has a steeper increase of the mean film thickness with increasing liquid load. An explanation could be that the chain elements are fixing liquid beads which grow with increasing liquid load but do not move downward (see Figure 2a). The plot in Figure 7c shows the significant reduction of the mean film velocity by the chain structures compared to the cylindrical wire.

Interfacial area

Figure 8 shows the specific interfacial area which was calculated with the film dimension data according to

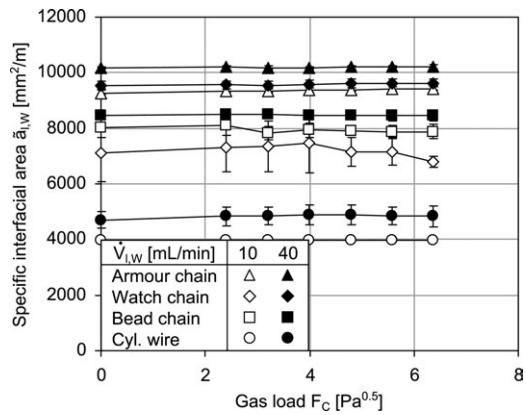

Figure 8. Specific interfacial area against gas load at varying liquid loads for different wire geometries.

Error bars: Standard deviation.

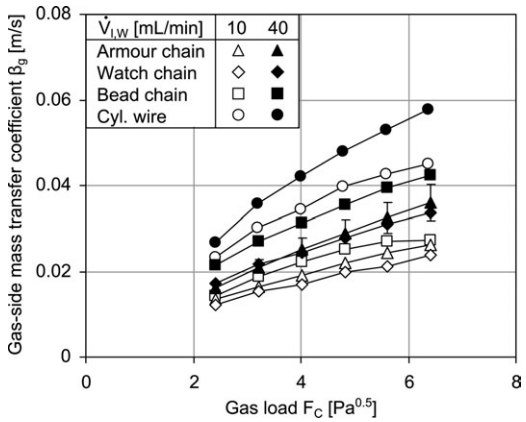

Figure 9. Gas-side mass-transfer coefficient over gas load for different wire geometries and liquid loads.

Error bars: Standard deviation exemplified for the armor chain.

Investigated structured wires section. It is plotted against the gas load for different wire geometries and varying liquid loads. It reveals that there is only a minor influence of the gas load on the interfacial area. Compared to the cylindrical wire, the chain geometries offer higher interfacial area per length. When comparing these results with the specific dry area given in Table 1, the example of the armor chain shows that the interfacial area is not necessarily higher than the dry surface area. This is caused by the fact that the liquid does not wet the armor chain to its whole extent and forms a relatively smooth surface (see Figure 2c).

Gas-side mass transfer

In Figure 9, the gas-side mass-transfer coefficient is plotted against the gas load for different chains and liquid loads. With increasing gas load, the mass-transfer coefficients are rising. An increase of the liquid load leads to higher mass-transfer coefficients which can be ascribed to the higher-relative velocity at the interphase and turbulent fluctuations. This also explains why the cylindrical wire shows the highest mass-transfer coefficients because the fast running beads intensify the mass transfer.

Figures 10a, b show the gas-side Sherwood number against the Reynolds number for the watch chain and the bead chain, respectively, for different liquid loads. The experimental results are compared with a correlation of Braun and Hiby[8] for planar film flow

$$Sh_g = 0.015\, Re_g^{0.75} Re_l^{0.16} Sc_g^{0.44} \left[1 + 5.2 \left(\frac{L_W}{b_C}\right)^{-0.75}\right] \quad (15)$$

and a correlation of Bravo et al.[9] for structured packings

$$Sh_g = 0.0338\, Re_g^{0.8} Sc_g^{0.333} \quad (16)$$

The Braun and Hiby correlation includes the dependency of the liquid Reynolds-number Re_l. It appears that the mass-transfer behavior of the watch chain follows the correlation of Braun and Hiby[8] more than the correlation of Bravo et al.[9] At least at high-liquid flow rates, the bead chain shows mass-transfer conditions similar to those of packed columns. This difference can be explained by the dominant flow pattern on the chain geometries: For the watch chain, no bead movement can be observed, whereas the bead chain develops a streak-like film flow pattern which intensifies the mass transfer.

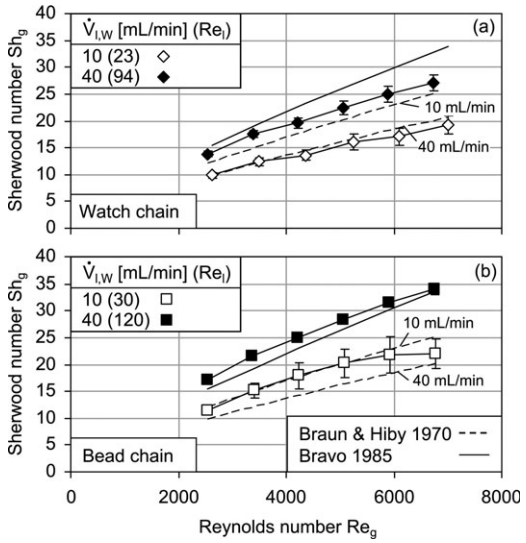

Figure 10. Gas Sherwood number over gas Reynolds number at different liquid loads for (a) watch chain and (b) bead chain.

Error bars: Standard deviation.

Estimation of Packing Separation Performance

To achieve a comparable specific surface area compared to common structured packings, the wires in the packing have to be packed with a certain density. Table 2 shows the proposed wire packing properties when assuming a quadratic spacing of 5 mm (z_P = 40,000 1/m^2) for the different wire geometries. In addition, the properties of a Montz B1-250 CSSP of comparable specific surface area are added to the table (values calculated with the model of Rocha et al.[10]).

As the test channel with the single chains has a higher-void fraction, the experimental data has to be adapted to the proposed wire packing geometry. When assuming equal effective gas velocities $\overline{w}_g$ in both the channel and the packing, the packing gas load has to be corrected as

$$F_P = F_C \frac{\varepsilon_P(1 - h_{l,P})}{\varepsilon_C(1 - h_{l,C})} \quad (17)$$

The dry packing area and the effective interfacial area of the packing are calculated as

$$a_P = \tilde{a}_W z_P \quad \text{and} \quad a_{l,P} = \tilde{a}_{l,W} z_P \quad (18)$$

Table 2. Proposed Wire Packing Properties for Different Chain Geometries (Quadratic Spacing 5 mm, z_P = 40,000 1/m^2)

	B_P, m^3/(m^2 h)			24		96	
	a_P m^2/m^3	ε_P	A_P/V_P 10^3 m^2/m^3	$a_{l,P}$ m^2/m^3	$h_{l,P}$	$a_{l,P}$ m^2/m^3	$h_{l,P}$
Watch chain	284	0.94	5.0	298	0.090	384	0.22
Armor chain	510	0.87	4.0	375	0.11	408	0.21
Bead chain	222	0.91	2.6	316	0.13	338	0.17
Cyl. wire (ø 1 mm)	126	0.97	4.0	160	0.022	195	0.048
Montz B1–250 CSSP	244*	0.98*	12.2	244†	0.04†	244†	0.08†

*Values taken from Olujić et al.[11]
†Values calculated with model of Rocha et al.[12]

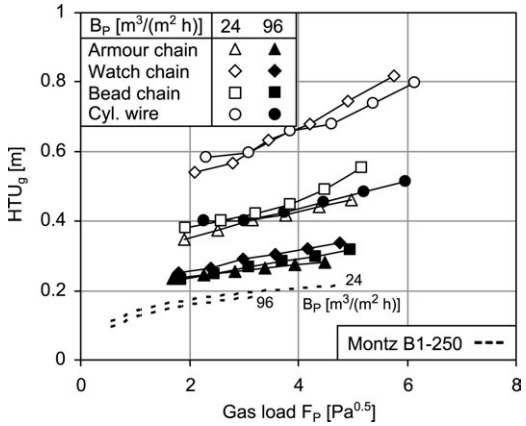

Figure 11. HTU_g-values for different wire packings depending on the gas load for different liquid loads.

Comparison with CSSP Montz B1-250 (model data from Rocha et al.[12]).

the packing void fraction and the liquid fill factor are calculated as

$$\varepsilon_P = 1 - A_{CSA,W} z_P \quad \text{and} \quad h_{l,P} = HU_{l,W} z_P / \varepsilon_P \tag{19}$$

The utilization of the packing material, expressed as the packing surface area related to the packing volume, is also shown in Table 2

$$A_P/V_P = a_P/(1 - \varepsilon_P) \tag{20}$$

For the geometries which consist of cylindrical wire elements such as the armor chain, watch chain, and the cylindrical wire itself, this relation is simply $A_P/V_P = 4/d_W$. Table 2 shows that the specific packing surface area a_P of the chains is enlarged significantly compared to the cylindrical wire packing at the cost of a reduced void fraction ε_P. However, the effective interfacial area of the chain and cylindrical wire packings is strongly depending on the liquid load B_P. In the case of the cylindrical wire and the watch chain, the effective interfacial area is higher than the dry packing surface area, whereas the armor chain shows the opposite behavior like discussed for the single wires in Liquid holdup Section. In contrast, the interfacial area of an irrigated CSSP is practically equal to the dry packing surface area at higher-liquid loads according to Olujić et al.[11]. However, the CSSP has the highest surface area per packing volume which means that less packing material is needed to achieve a certain surface area.

The HTU_g-values of different wire packings are presented in Figure 11 for varying liquid loads. For comparison, the trend of a Montz B1-250 CSSP is also plotted (calculated with the model from Rocha et al.[12]). Different gas load ranges of the data result from the corrected packing gas load calculated with Eq. 17 and indicate the operating range. It is apparent that the wire packings have a higher-load capacity than the CSSP. Opposite to the CSSP, the wire packings show a strong dependency of the liquid load which results from the varying interfacial area (see Table 2) and mass-transfer coefficients (see Figure 9). It is remarkable that the chain packings have a similar characteristic at high-liquid loads ($B_P = 96$ m³/(m² h)). However, the CSSP has the lowest HTU_g-values which can be explained by the structure of the packing. As the gas channels in the packing are inclined in an angel of 45° to the main gas flow direction, the mass-transfer coefficients are higher due to increased effective gas velocities in the gas channels. Conversely, his advantage is bought dearly with a higher-pressure drop per packing height.

Conclusions

The experimental results show that a liquid film can be stabilized by appropriate wire geometries such as chains. As a consequence, load limits increase but the mass-transfer coefficients are lower than for the cylindrical wire. Conversely, the interfacial area is enlarged using chains. In the proposed packing configuration, this leads to higher-separation efficiencies. The wire packings are supposed to have advantages in the field of phase distribution, loading range, and specific pressure drop. The common CSSP show lower-maximum loading rates but offer better utilization of the packing material and are easier to manufacture and to install. Therefore, a further optimization of the geometry should focus on these issues.

Acknowledgments

The authors gratefully acknowledge the financial support of the Deutsche Forschungsgemeinschaft DFG (German Research Foundation) for this work (Project no. KR1639/13-1).

Notation

A = area, m²
$a_{l,P}$ = specific effective interfacial area in the packing, m²/m³
$\tilde{a}_{l,W}$ = specific film surface area on wire, referred to wire length, m²/m
a_P = specific surface area of the dry packing, m²/m³
b_C = cross-sectional dimension of the channel, m
$B_P = \dot{V}_l/A_{CSA,P}$ = liquid load of the packing, ref. to cross-sectional area, m³/(m² h)
$B_W = \dot{V}_{l,W}/\tilde{a}_W$ = liquid load of wire, ref. to the specific wire surface area, m³/(m h)
D = diffusion coefficient, m²/s
d_h = hydraulic diameter of the gas passage, m
d_W = diameter of wire, m
e = local width of liquid film, m
$F = v_g \rho_g^{0.5}$ = gas load, F-factor, Pa^0.5
$h_l = V_l/(\varepsilon V_{tot})$ = liquid fill factor, -
HTU_g = height of a gas-side transfer unit, m
$HU_{l,W} = V_{l,W}/L_W$ = liquid holdup on the wire, mL/m
l = chain link dimension, m
L_W = length of wire, m
L_{sin} = arc length of sinus function, m
N_{CL} = number of chain links, -
$\dot{N}$ = molar flow rate, mol/s
p = pressure, Pa
$p_{air,m}$ = mean partial pressure of inert gas (air), Pa
p_{H_2O} = partial pressure of H_2O in the gas phase, Pa
$p_{H_2O,ln}$ = logarithmic partial pressure difference, Pa
R = universal gas constant, J/(mol K)
$Re_g = \overline{w}_g d_h/\nu_g$ = gas Reynolds number
$Re_l = B_W/\nu_l$ = liquid Reynolds number, -
$Sc_g = \nu_g/D_g$ = gas Schmidt number, -
$Sh_g = \beta_g d_h/D_g$ = gas Sherwood number, -
T = temperature, K
v = superficial velocity, m/s
$\dot{V}$ = volume flow rate, m³/s
V = volume, m³
$\overline{w}_g$ = mean gas velocity, m/s
$\overline{w}_{l,f}$ = mean liquid film velocity, m/s
z_P = packing density of wires per cross sectional area, 1/m²

Greek letters

β_g = gas-side mass-transfer coefficient, m/s
δ_m = mean film thickness, μm
ε = void fraction, -
ν = kinematic viscosity, m²/s

Abbreviation

CSSP = corrugated sheet structured packing

Sub- and superscripts

* = equilibrium
C = channel
CSA = cross sectional area
g = gas
I = interphase
l = liquid
ln = logarithmic
m = mean
P = packing
tot = total
W = wire

Literature Cited

1. Sperandio A, Richard M, Huber M. Eine neue Packung für die Vakuumrektifikation.*Chem Ing Tech*.1965;37:322–328.
2. Stikkelman R, de Graauw J, Olujić Ž, Teeuw H, Wesselingh H. A study of gas and liquid distributions in structured packings. *Chem Eng Technol*. 1989;12:445–449.
3. Hattori K, Ishikawa M, Mori YH. Strings of liquid beads for gas-liquid contact operations. *AIChE J*. 1994;40:1983–1992.
4. Grünig J, Skale T, Kraume M. Liquid flow on a vertical wire in a countercurrent gas flow. *Chem Eng J*. 2010;164:121–131.
5. Thomsen K. Approximate solution for ellipsoid surface. 2004;http://www.numericana.com/answer/ellipsoid.htm#thomsen. Accessed 28.03.2011.
6. Gilliland ER, Sherwood TK. Diffusion of vapors into air streams. *Ind Eng Chem*. 1934;26:516–523.
7. VDI/VDE Richtlinien, ed. *VDI 3514 Part 1: Measurement of humidity—Characteristics and symbols*. Berlin: Beuth Verlag,2007.
8. Braun D, Hiby JW. Der gasseitige Stoffübergangskoeffizient am Rieselfilm (in German). *Chem Ing Tech*. 1970;42:345–349.
9. Bravo JL, Rocha JA, Fair JR. Mass-transfer in gauze packings. *Hydrocarb Process*.1985;64:91–95.
10. Rocha JA, Bravo JL, Fair JR. Distillation-columns containing structured packings—a comprehensive model for their performance.1. Hydraulic Models. *Ind Eng Chem Res*. 1993;32:641–651.
11. Olujić Ž, Kamerbeek AB, de Graauw J. A corrugation geometry based model for efficiency of structured distillation packing. *Chem Eng Process*. 1999;38:683–695.
12. Rocha JA, Bravo JL, Fair JR. Distillation columns containing structured packings: a comprehensive model for their performance. 2. Mass-transfer model. *Ind Eng Chem Res*. 1996;35:1660–1667.

Manuscript received July 27, 2011, and revision received Mar. 3, 2012.